Multi compression–expansion process for chemical energy conversion: Transformation of methane to unsaturated hydrocarbons and hydrogen

Simon Drost [*], Robert Schießl, Ulrich Maas

Institute of Technical Thermodynamics, Karlsruhe Institute of Technology (KIT), 76131 Karlsruhe, Germany

ARTICLE INFO

ABSTRACT

With the global energy system moving towards renewable energies, there is an increasing demand for flexible conversion processes which can cope with the temporally and locally fluctuating nature of energy supply and energy demand. Promising candidate processes are based on coupled chemical/energy conversion. In this work, the pyrolytic conversion of methane to valuable high-energy content substances like hydrogen and unsaturated hydrocarbons by the compression/expansion process of a piston engine is investigated. In particular, the potential of running this conversion in a multi-compression–expansion (MCE) mode where a gas sample is subject to multiple compression–expansion strokes, is assessed. The methane conversion and target species yields of this multi-compression mode relative to a single compression–expansion mode are assessed. Experimental studies with a rapid compression–expansion machine are used for this. The experiments are complemented by numerical simulations, which help to interpret the experimental findings. We found that both conversion and target species yields can be increased significantly by the multi-compression–expansion processes relative to a single compression–expansion. For instance, at typical engine operation conditions, ten compression–expansion cycles increase the methane conversion by a factor of three to four (from approx. 15 % to 68 %), the hydrogen yield by a factor of five, and the unsaturated hydrocarbon yields by a factor of three, compared to a single compression–expansion process. The results encourage considering a new role for piston-engines as work-to-chemical energy converters, in addition to their conventional heat-engine (chemical energy to work) operation.

1. Introduction

Surplus energy, for example from wind and solar energy devices, can be employed to run chemical processes that produce some desired valuable chemical species [1,2]. One example is the conversion of methane (CH_4) into hydrogen (H_2) and/or unsaturated hydrocarbons (UHC, e.g., C_2H_2 and C_2H_4) via high-temperature paths [3,4]. For these systems, a reaction path analysis is performed by [3]. The products are superior to the reactant (CH_4) both in their economic value and in their content of free energy. In addition, CH_4 as a main component of natural gas has been intensively studied and is already well investigated [5,6]. This endothermal conversion cannot run spontaneously at standard conditions for reasons of both equilibrium chemistry and chemical kinetics. It can be stimulated, however, by input of mechanical work in reciprocating piston engines, as has been demonstrated, e.g., in [7–9].

Using piston engines as chemical energy converters offers several benefits. First, after more than a century of development, piston engines are now reliable, robust and mechanically highly efficient machines, capable of operation under adverse conditions like extremely high temperatures and pressures. Their operation also covers a large range of converted power and mass flow rates. Importantly, a piston engine can also meet temporally varying power demands within timescales of seconds. Process chains for producing and maintaining piston engines are well established and efficient. Much of the know-how and infrastructure developed for piston-compressor based heat engines can be exploited also for piston-compressor based energy converters.

Also, the total number of piston engines worldwide is huge, exceeding one billion. With the phase-out of their conventional use as combustion-based heat engines, a flood of retired piston engines will become available for alternative uses. A new employment as chemical reactors helps to make economic use of the huge amount of existing engines. In addition, piston engines offer excellent size scalability, which is a critical factor in the practical use of energy conversion systems. Piston engine sizes, expressed in displaced volume, range from below one liter to thousands of liters, easily spanning three orders of magnitude. Together with the wide range of accessible revolution speeds (typically spanning a factor of 10 for one engine), the pool of

---

* Corresponding author.
  E-mail address: simon.drost@kit.edu (S. Drost).

existing piston engines offers several orders of magnitude in realizable mass flows, and thus, a similarly huge range of realizable conversion power and mass flows.

The question for piston engine operation parameters that maximize the desired outputs of the conversion naturally appears. Common parameters that influence the chemical reactions (e.g. conversion and yields) during a compression process are the initial pressure, initial temperature, compression ratio and the initial mixture composition [10–12]. Many elementary reaction steps underlying the desired conversion have high activation energies, and thus, high temperatures are required to initiate reactions. Also, the conversion from methane to a hydrogen/UHC mixture is strongly endothermal; reaction equilibria can therefore be shifted to the desired products by providing high temperatures. Overly high temperatures, however, may cause the desired unsaturated hydrocarbons to react further to soot or soot precursors. The yields of substances like acetylene and ethylene are therefore limited both by too low and too high temperature [13–15].

The CH_4 conversion depends on the chemical kinetics and the residence time in the high-temperature phase of a compression/expansion process. This residence time dependence suggests that the conversion can be enhanced by rendering the shape of the volume history such that a long high temperature phase is provided. Additionally, dilution of the reactants with noble gases can be used to obtain the required high temperatures. However, the endothermic reaction leads to a fast temperature decrease [16]. Heat losses of the compressed hot gases to the cylinder walls tend to lower the gas temperatures. With the reduced temperature, the endothermic reaction of the CH_4 conversion also practically stops. A longer hold time of the piston at TDC therefore has no further advantage with regard to CH_4 conversion. The conditions of too low temperature can be overcome by additional compressions of the reacted gas to increase the gas temperature again. By repeated compressions, higher CH_4 conversions can be achieved by an incrementally progressing reaction in comparison to a single compression.

In this work, we study the potential of multi-compression–expansion (MCE) operation modes for improving CH_4 conversion and product species yields, in comparison to a single compression. The study is based on Rapid Compression–Expansion Machine (RCEM) experiments in which conversion and yields during repeated compression–expansion cycles are measured. The experimental results are accompanied by numerical simulations, which serve as an aid to interpret the experimental findings. This is followed by a feasibility study to show the potential of the process for realistic reciprocating engines. Results indicate that the multi compression–expansion process can significantly increase the conversion and yields compared to a single compression process. For the studied conditions, conversion enhancement of up to a factor of 5 compared to was found. Furthermore, the multi compression–expansion process can reach yields that would be hard to reach in single stroke operation because of the forbiddingly high required temperature levels.

2. Methodology

2.1. Experimental methods

2.1.1. Rapid Compression–Expansion Machine (RCEM)

The Rapid Compression–Expansion Machine (RCEM), a piston-cylinder device similar to a piston engine, is described in [17–20]. Therefore, only the most important key points are mentioned here.

The RCEM is operated in a configuration where after the compression stroke, the piston is first held at top dead center (TDC) position for a certain, pre-determined hold time τ_H. τ_H is adjustable and typically set to values above 5 s. After the hold time, expansion can be performed by moving the piston back to bottom dead center (BDC). During the whole compression-hold-expansion-process, no mass exchange take place. At BDC, the piston again is held at fixed position, for a period that is long enough to allow the gas in the cylinder to attain a stationary and homogeneous thermodynamic state.
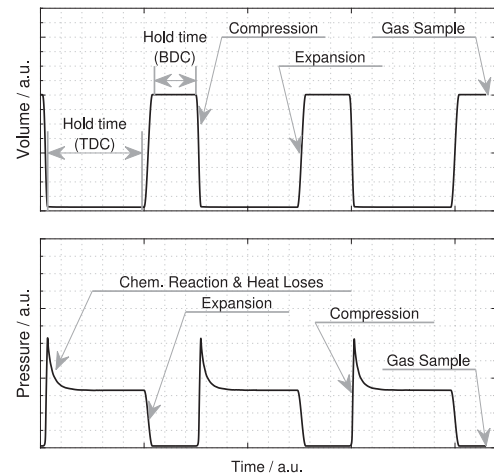

Fig. 1. Sketch of volume (top) and pressure (bottom) curves with three compression–expansion cycles in the RCEM configuration without gas exchange between the cycles.

Contrary to the common use of a creviced piston, a flat-head piston is used; the adiabatic/isentropic core assumption is valid only a few ms after compression [21]. This allows to achieve higher compression ratios, and thus, higher compression temperatures, compared to a creviced piston. As a representative temperature associated with a compression event, the isentropic core temperature, was determined from the experimental pressure trace and the pre-compression temperature, assuming an isentropic relation between p and T. This temperature is a basis for comparing results between different experiments, and also between experiment and simulation.

The investigated gas mixture consists of 5/90/5 CH_4/Ar/He (molar) with the purities 99.995% (CH_4), 99.996% (Ar), and 99.996% (He).

The gas mixture was produced according to the partial pressure approach in a mixing chamber with a volume of approx. 20 l. The static pressure during the preparation of the mixture as well as the total pre-compression pressure was measured with a MKS Baratron 121A [22]. The accuracy of reading is $U_{p0} \leq \pm 0.5\%$. The dynamic pressure was measured in the combustion chamber using a Kistler 6061 B sensor [23]. The full scale output was adjusted to 40 bar with a linearity of $U_{p(\tau)} \leq 0.5\%$. The stroke was measured with a potentiometric displacement transducer (Burster Typ 8712 [24]). The full scale output was adjusted to 100 mm with a non-linearity of $U_S \leq 0.1\%$. The static temperature before compression was measured with a type K thermocouple with an accuracy of 2.2 K. Gas analysis was performed with a gas chromatograph (GC), model Agilent 490 Micro GC [25,26].

2.1.2. Experimental procedure

A multi-compression experiment is performed in the RCEM by compressing and expanding the cylinder load several times, without gas exchange between the compression/expansion cycles. Besides the initial values of pressure, temperature and gas composition, as well as the compression ratio, other parameters influencing the CH_4 pyrolysis are the volume curve and the times at which valves are opened and gas exchange takes place. The volume curve itself is characterized by the compression ratio and the duration of the compression- and expansion-stroke, as well as the hold-time at TDC and BDC.

In the experiment, the 5/90/5 CH_4/Ar/He (molar) gas mixture is filled into the evacuated RCM's combustion chamber (with the piston resting in BDC position) until the desired initial pressure is reached. The valves on the combustion chamber are then closed; the gas mixture is compressed within approx. 30 ms, as shown in Fig. 1. The upper and lower part of Fig. 1 depict the volume and pressure history, respectively, during a typical compression process in the RCM. After reaching

TDC (maximum pressure in Fig. 1), the piston is fixed in this position and held for approx. $10\,s$ (Fig. 1, hold time). As long as the temperatures remain high during this hold time, CH_4 conversion proceeds. At the same time, heat losses occur, causing a temperature drop until finally the gas temperature reaches the cylinder wall temperature. Followed by the hold time at TDC, the piston is driven back to BDC (expansion). No valves are opened and the gas in the combustion chamber is not exchanged. After allowing the gas to homogenize for approx. $60\,s$ at BDC position, the experimental procedure repeats, adding a new compression - hold at TDC - expansion - hold at BDC - cycle, all still without any mass exchange. After a pre-defined number of K repetitions, the valve between the combustion chamber and the GC is opened and a sample of the reacted gas is analyzed in the GC. For the subsequent experiment with $K + 1$ compression–expansion cycles, the initial gas mixture 5/90/5 CH_4/Ar/He (molar) is filled in the evacuated combustion chamber and is compressed/expanded $K + 1$ times before the gas is analyzed in the GC.

2.2. Modeling

In the following subsections, first the RCEM/piston engine model will be presented.

2.2.1. RCEM/piston engine model

To account for temperature inhomogeneities in the combustion chamber, a multi-zone model (MZM) is employed. The MZM consists of several spatially distinct zones which are arranged in an onion-skin like fashion. Each zone is spatially homogeneous with respect to temperature, pressure and composition. There is no mass transfer between zones, and the pressure is the same in all zones $p_z = p_{z+1}$. A zone can transfer heat to its adjacent zones, and can deliver or accept expansion or compression work, respectively, to the gas outside of that zone. The inner zones in the model are assigned equal masses ($m_{z-1} = m_z$ with $z = 3, \dots, n_Z$) and equal heat transfer coefficients between the zones ($\alpha_{z-1} = \alpha_z$ with $z = 3, \dots, n_Z$), where n_Z is the total number of zones.

To make the sure the MZM provides a realistic description of the thermal condition in the RCEM combustion chamber, experimental pressure histories during the compression of an inert gas (Ar) were used to calibrate/adjust the following model parameters:

(a) the heat transfer coefficient α_1 between the boundary layer (outermost zone, $z = 1$) to the cylinder wall,
(b) the volume of the boundary layer V_1 (initial state),
(c) the heat transfer coefficients of the inner zones α_z with $z > 1$, and
(d) the number of zones n_Z.

The experimental data show that the RCEM is nearly perfectly gas tight ($p_0 V_0 \approx p_F V_F$, with index "0" denoting the pre-compression state and index "F" denoting the compressed state after complete heat transfer, with temperature $T_F = T_0$).

The following points are selected as supporting points for the calibration; the model parameters were adjusted such that these reference points were matched by the simulation. In the following, index "C" denotes the state at the end of the compression:

(a) maximum pressure near end of compression p_C,
(b) steady state pressure after compression and cooling (p_F)
(c) pressures at additional points between p_C and p_F,
(d) compression temperature T_C (determined by the adiabatic core assumption).

The matching of parameters is done numerically by minimizing the relative errors between the experimental and numerical supporting points. MATLAB's genetic algorithm (GA, [27–30]) was used for this. For the calculations, the experimental volume history of the RCEM was
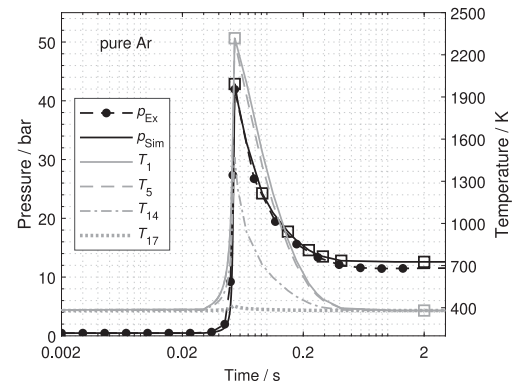

Fig. 2. Comparison of experiment and calibrated multi-zone model (17 zones) of pressure and temperature for a single compression. The relative deviation for the pressure (black squares) and for the temperature (gray squares) is less than 10%. Pressure curves (black) belong to the left y-axis, temperature curves (gray) belong to the right y-axis.
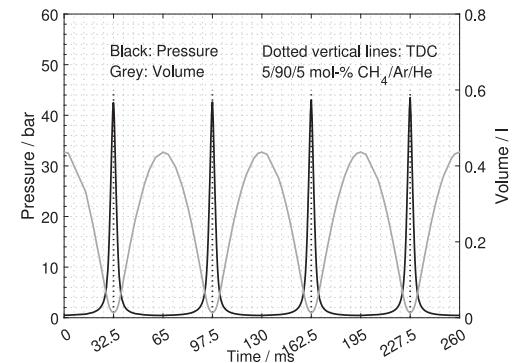

Fig. 3. Pressure and volume curve of a multi compression–expansion process simulation with an engine-type volume curve (no hold times) for four compression–expansion cycles.

used as input. Adjustments as done in other models, for example in an adiabatic/isentropic core model, were not applied. Fig. 2 shows an example of a fitted pressure curve and four temperature curves outermost zone ($z = 1$), two middle zone ($z = 7$ and $z = 10$) and the innermost zone ($z = 17$). The choice of 17 zones is also confirmed by Wilson et al. [31]. They performed a MZM grid study for RCMs and found that more than 15 zones did not significantly change the yields.

Piston engine model. The RCEM is a useful research device for tests under well-defined conditions. However, for the RCEM process, the hold phase at TDC causes higher heat losses near TDC and longer cycle times compared to a piston engine process. To, the model simulation is additionally run with an engine volume curve, with a speed of $960/min$ and a compression ratio of 29. An example of the pressure- and volume curve is shown in Fig. 3.

For a given volume curve $V(t)$, the compression work $W(t_F)$ is calculated as

$$W(t_F) = -\int_0^{t_F} p(\tau) \dot{V}(\tau) d\tau, \tag{1}$$

with the temporal derivative of the volume curve $\dot{V}(\tau)$ and the pressure $p(\tau)$. The integration starts at the initial point t_0 with the initial gas mixture and ends at time t_F; several compression–expansion cycles can occur in this time.

As a quantity describing the energetic benefit of the conversion process, the Gibbs free energy G is chosen. The difference ΔG between the reacted mixture (with species mole fractions $X_i(t), i = 1, \dots, n_s$ with the number of chemical species n_s) after some time t and the initial

(pre-compression) mixture (mole fractions $X_{i,0}$) is evaluated using the initial values p_0, T_0 of pressure and temperature:

$$\Delta G = \Delta H - T \Delta S \qquad (2)$$
$$= H(T_0, X_i(t)) - H_0(T_0, X_{i,0})$$
$$- T_0(S(p_0, T_0, X_i(t)) - S_0(p_0, T_0, X_{i,0}))$$

2.2.2. Reaction mechanism

For the simulations, two reaction mechanisms from the literature were employed in a comparative study. The first mechanism is a reduced version of the detailed NUI Galway reaction mechanism 1.1 (NUIGMech 1.1, 2746 species, 11 279 reactions [32–42]), with all reactions containing species with O- or N- atoms removed from the detailed version. The reduced reaction mechanism consists of 320 species and 1518 reactions.

The second mechanism is a relatively small C1-C4 reaction mechanism, developed for aromatic and polycyclic aromatic hydrocarbon combustion (LLNL C1-C4, 155 species, 689 reactions, [43]).

2.2.3. Numerical solution

The equations for the multi-zone model are solved numerically by the in-house code HOMREA [44], which simulates the chemical-physical state in the combustion chamber using a predefined volume profile.

3. Results

The results are divided into two sub-sections. The first sub-section compares CH_4 conversion and species yields from RCEM experiments with simulations. The second sub-section is a feasibility study that models the process with the volume curve of a reciprocating engine (compression/expansion without the hold phases of the RCEM).

3.1. RCEM experiments and simulations

As mentioned, there is a long hold time during which the piston is held in bottom dead center position between different compression–expansion cycles. The hold time at BDC is chosen long enough (approx. 60 s) to allow a complete homogenization of the gas in the combustion chamber.

Fig. 4 shows the CH_4 conversion over the number of cycles for the RCEM experiments and for simulations with the reduced NUIGMech 1.1 and the LLNL C1-C4 reaction mechanism.

The CH_4 conversion $C^{(K)}$ after K cycles

$$C^{(K)} = 1 - \frac{n_{CH_4,1}^{(K)}}{n_{CH_4,0}^{(1)}} \qquad (3)$$

is determined from the molar amount of CH_4, $n_{CH_4,0}^{(1)}$ before the first compression–expansion cycle ($K = 1$, index 0) and the molar amount $n_{CH_4,1}^{(K)}$ after K cycles. The experiments and simulations are performed at an initial pressure $p_0 = 0.5$ bar, an initial temperature $T_0 = 380$ K and a compression ratio $CR \approx 29$.

The diagram shows that CH_4 conversion increases with the number K of compression–expansion cycles; the increase is strong at the first compressions. For $K < 4$, the conversion increases by about $c \approx 0.15$ each cycle. After 5 cycles, half of the initial methane is converted. At $K = 10$ cycles, the experiments showed a total conversion of $C^{(10)} = 0.7$. The simulations show almost the same conversion as the experiments for the first cycles, especially the NUIGMech 1.1. With increasing number of cycles K, the difference between experiment and simulation increases, with the simulations showing slightly higher conversion levels than the experiment. The final conversion after 10 cycles is near 80% for both reaction mechanisms. Both the experiment and
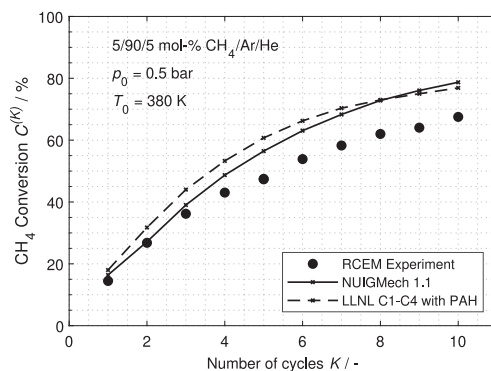

Fig. 4. Total CH_4 conversion $C^{(K)}$ after K cycles for RCEM experiments and simulations. Simulation results are shown as lines to guide the eye. Full line: NUIGMech 1.1 reaction mechanism [32–42]. Dashed line: LLNL C1-C4 with PAH reaction mechanism [43].

the simulations show that the CH_4 conversion is increased by a factor of 4–5 by the multi compression–expansion process in comparison to a single compression process.

The increase in CH_4 conversion is non-linear and becomes less pronounced with increasing K (Fig. 4). The total amount of CH_4 converted after K cycles, with $K > 1$ is lower than if the cylinder is refilled each time. However, the multi-compression process can achieve very high CH_4 conversions, that cannot be realized with a single compression. The high CH_4 conversion has additional advantages, e.g. allowing easier separation of the species or higher stored energy densities. The stored energy density achieved by complete conversion from methane to a hydrogen/acetylene mixture, expressed as standard Gibbs free energy increase between the product mixture and the initial reactant per mass of reactant, is 9 MJ/kg. The RCEM experiments indicate that stored energy densities above 2 MJ/kg (per 1 kg CH_4) (about twice the values of e.g., Li-Ion batteries [45]) are readily achieved, even without any attempt to optimize conditions for energy storage.

With multi-compression operation, CH_4 conversions $C \approx 0.68$ have been demonstrated in our experiments, at an initial temperature $T_0 = 380$ K. Such a moderate initial temperature is well feasible for engine operation. In contrast, with single-compression operation, similarly high conversions could be realized only with extremely high initial temperatures; simulations show that, even with $T_0 = 800$ K, single-compression conversion does not exceed $C = 0.35$.

Thus, the multi-compression cycle can achieve conversions in a piston engine that are difficult to achieve with only a single compression.

The yield Y_i of species i [46] is defined as the ratio of the actual amount of i and its maximum possible amount at the atomic composition given by the initial reactants. For a MCE process, we can define the yield after the Kth cycle by:

$$Y_{i,K} = \frac{n_{i,1}^{(K)}}{\max(n_i)} = \frac{n_{i,1}^{(K)}}{\nu_i n_{CH_4,0}^{(1)}} \qquad (4)$$

Here, ν_i is the stoichiometric coefficient in the reaction forming species i from CH_4, e.g. $CH_4 \rightleftharpoons \nu_{C_2H_2} C_2H_2 + 1.5H_2$ with $\nu_{C_2H_2} = 0.5$.

The yields of H_2, C_2H_2 and C_2H_4, for RCEM experiments and simulations, are shown in Fig. 5. It is observed that the yield of H_2 increases strongly with the number of cycles. Both reaction mechanisms predict this trend well, even with good quantitative agreement. For C_2H_2 and C_2H_4, experimental yields increase for the first 4 cycles, but remain constant during later cycles. Both yields are however, significantly larger after 10 cycles than after a single cycle.

The model simulations using the LLNL C1-C4 reaction mechanism predict similar yields for C_2H_2 and C_2H_4. The yields obtained with a model based on the NUIGMech 1.1 mechanism differ from this in that they predict higher yields for C_2H_2 than for C2H4. This relation between
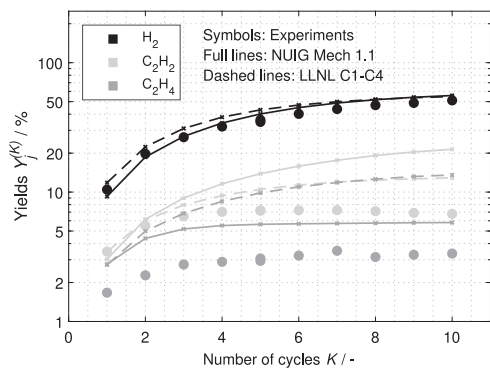
Fig. 5. Yields for H_2, C_2H_2 and C_2H_4 each after K cycles. Simulations are shown as lines to guide the eye. Full line: NUIGMech 1.1 reaction mechanism [32–42]. Dashed line: LLNL C1-C4 reaction mechanism [43]. The Y-axis is plotted logarithmically for better readability.

Fig. 6. Mole fractions weighted with the number of C atoms as a function of number of cycles (simulations). Species are classified in three groups according the number of C atoms. Full line: NUIGMech 1.1 reaction mechanism [32–42]. Dashed line: LLNL C1-C4 reaction mechanism [43]. No experimental data as the GC is not configured for these species.

the yields is consistent with the experiments. A good agreement between the experiments and simulations performed with the NUIGMech 1.1 is found for the C_2H_4 yields.

Motivated by the difference between modeling and experimental results regarding the C_2H_2 and C_2H_4 yield, further investigations are carried out. A possible explanation for the deviation of experiments to the NUIGMech 1.1 based simulations could be the absence of important reactions forming polycyclic aromatic hydrocarbons (PAHs). In order to investigate the different C_2H_2 production paths of the reaction mechanisms, the mole fractions of the other product species are studied first.

Besides C_2H_2, C_2H_4 and H_2 many other species are produced with a mole fraction $>5 \cdot 10^{-6}$ (chosen limit). For simplification, the species are summarized in three groups: (a) C_2 - C_4 species, which usually do not form aromatic rings, such as butatriene (C_4H_4). The species CH_4, C_2H_2, and C_2H_4 are excluded. (b) C_5 - C_8 species, including aromatic compounds. In this group, benzene (C_6H_6) is the main species, but also e.g. toluene ($C_6H_5CH_3$) is produced. (c) The third group includes species with more than one aromatic ring, called $>C_8$, with indene (C_9H_8) as one of the first representatives. The summarized mole fractions weighted by C atoms of each species of these three groups are shown in Fig. 6 over the number of cycles. Other small hydrocarbons than CH_4, C_2H_2, and C_2H_4 are only present in small quantities (light gray lines close to zero) for both reaction mechanisms. The results of the second group with C_5 - C_8 species looks similar, however, there is a difference in C_6H_6 by almost a factor of two, with LLNL C1-C4 reaction mechanism predicting a higher value. In the third group, primarily PAHs, the greatest discrepancy between the two mechanisms is found. The C atom balance derived from the experimental values of (C_2H_2, C_2H_4) and CH_4 shows a deficit relative to the initial mixture, which points to the presence of experimentally undetected carbon-containing species. The carbon deficit increases with the number of cycles. After the first cycle, more than 90% of the original C atoms are found in detected species, while this fraction has dropped to 43% after 10 cycles. If only the C atoms of the species CH_4, C_2H_2 and C_2H_4 are counted in the simulation, a similar deviation and trend is observed. This can explain the stagnating C_2H_2 and C_2H_4 yields after a view cycles, while constantly increasing CH_4 conversion.

3.2. Feasibility study

The previous sub-section showed that the two reaction mechanisms we employed for the simulation studies, although not developed specifically for pyrolytic conversion of methane in multiple compression–expansion processes, predict the trend (and often also the values) of the
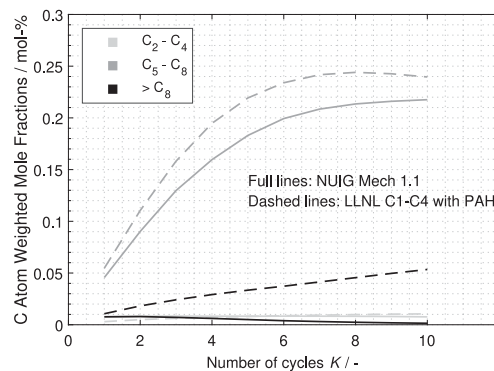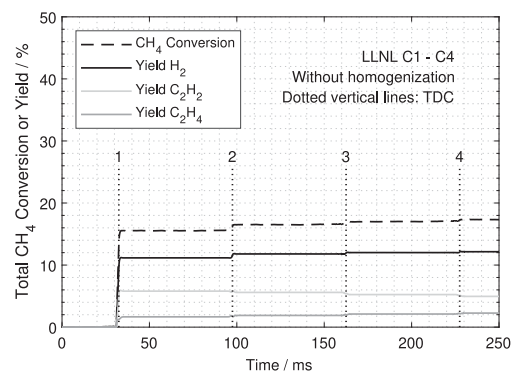

Fig. 7. Time-resolved CH_4 conversion and H_2, C_2H_2, and C_2H_4 yields over four compression–expansion cycles with engine type volume curve. Simulations are performed without mass exchange between the zones.

CH_4 conversion and the target species yields reasonably well. Therefore, the reaction mechanisms and the model are used for a numerical study of the feasibility of this process reciprocating engines. The engine model described above (specifically, the same heat loss parameters and same distribution of zones).

Fig. 7 shows the time-resolved CH_4 conversion and species yields during four compression–expansion cycles. In these simulations, each zone of the MZM-model kept its contained mass between different cycles, i.e., no mixing between different zones was included in the model. In the first cycle, the result is comparable with the RCEM results. However, in the engine-type simulation, the conversion increases only sightly with additional cycles. This can be explained by the non-existing mixing between the zones. In the outer zones/layers, which are strongly affected by wall heat losses, almost no chemical reaction is observed because of the generally low temperature levels in those zones.

For multiple compression–expansion cycles in reciprocating engines, this stratification will decay by internal flow and mixing processes in the combustion chamber. In the model, this homogenizing effect can be included by assigning the combustion-chamber wide mass-averaged thermodynamical state to all zones between cycles.

CH_4 conversions and yields predicted by simulations with homogenization included (based on the LLNL C1-C4 reaction mechanism) are shown in Fig. 8. With the homogenization after each cycle, the CH_4 conversion and the yield increase with the number of cycles, in a fashion that compares well to the RCEM experiments. This shows that simulations of the multi-cycle conversion in engines require a consideration of mixing processes in the cylinder to be realistic. Due to heat losses and the endothermic reaction, the temperature at the
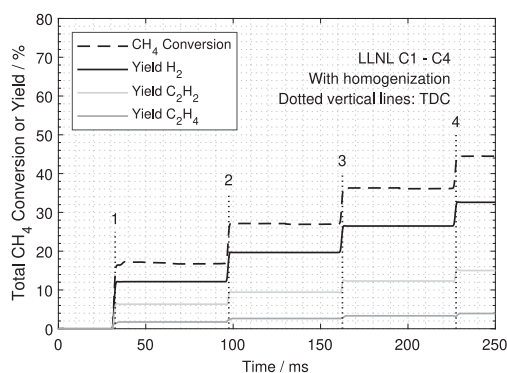
Fig. 8. Lines: Time-resolved CH_4 conversion and H_2, C_2H_2, and C_2H_4 yields over four compression–expansion cycles with engine type volume curve. Simulations are performed with homogenized mixtures after each cycle.
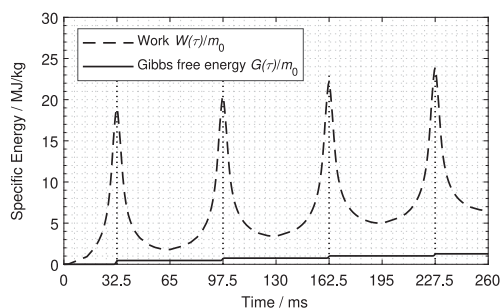

Fig. 9. Time-resolved specific mechanical work (Eq. (1)) transfer to the gas and increase of the specific Gibbs free energy (Eq. (2)).

end of a compression–expansion cycle is lower than the cylinder wall temperature. At the BDC phases between multiple cycles, the heat flow direction is reverse to the usual engine pattern, namely from the walls to the gas. The yields and the CH_4 conversion achieved with the engine type volume curve are comparable to the RCEM results also quantitatively. The CH_4 conversion with the underlying engine type volume curve is a little lower because the temperature decreases faster after reaching TDC due to the expansion. The comparison between RCEM vs. engine type volume curve and homogenization vs. without homogenization shows, that the mass transport in the cylinder has a greater influence than the volume curve.

One use of the multi compression–expansion process can be energy storage. Fig. 9 shows the evolution of energy related quantities during a multi compression–expansion process with homogenization of the mixture after each cycle. The work $W(\tau)$ shown is the total work transferred by the piston to the gas up to time τ. From BDC to TDC work is transferred to the engine, between TDC and BDC, work is transferred from the engine: Initially (time $\tau = 0$, BDC), $W(\tau)$ transferred to the gas increases by compression. After reaching TDC (vertical dotted line), work is transferred from the gas. In an ideal, adiabatic case without reaction, the net work transfer over a whole cycle would be zero. With heat losses and endothermic reaction included, the net transferred work does not reach 0 after one cycle is completed ($\tau = 62.5$ ms). The Gibbs free energy G increases with each cycle. In the example shown here, mass-specific G rises to a value near 1 MJ/kg within 230 ms (four cycles).

4. Conclusions

In this work, the use of piston engines as reactors for chemical energy conversion processes is studied. Specifically, the multi

compression–expansion (MCE) operation mode for piston engines performing a pyrolytic conversion of methane into unsaturated hydrocarbons and H_2 is studied experimentally and numerically. In MCE mode, the piston engine applies several subsequent compression–expansion cycles to a gas sample, without gas exchange between the cycles. It turned out that with increasing number cycles in a MCE-process, the CH_4 conversion and the target species yields can increase in comparison to a single compression–expansion cycle. This increase can be quite significant; for instance, after ten compression–expansion cycles the methane conversion can be increased by a factor of three to four, hydrogen yield by a factor five and yields of unsaturated hydrocarbons by a factor three. This was confirmed both in RCEM experiments and in simulations. The numerical model reproduced the experimental values of methane conversion as well as the H_2 and C_2H_4 yields well. In particular, the first cycles generally showed good agreement between experiment and simulation. With increasing number of cycles, the difference for the C_2H_2 yield between experiment and simulation as well as between the numerical results with different reaction mechanisms became larger. In addition, the species histories in multi compression–expansion cycles can be a test case for reaction mechanism validation. The multi compression–expansion operation mode for piston-engine type chemical converters offers several advantages over single compression: Compared to a single cycle, higher yields of the target species in the exhaust gas can be achieved. These high yields are hard to achieve in single compression mode, since very high temperatures would be required for this. The higher target species yields are also favorable for further process steps of the product gas, like e.g., the separation of pure species from the mixture.

In numerical investigations, it was not possible to obtain such high CH_4 conversions in a single compression even with an initial temperature of 800 K, highlighting the benefit of the multi compression–expansion process. In addition, in multi-compression mode, the CH_4 conversion gets divided into a sequence of incremental partial CH_4 conversions. This offers additional insights into the chemical kinetics.

Declaration of competing interest

The authors declare that they have no known competing financial interests or personal relationships that could have appeared to influence the work reported in this paper.

Data availability

Data will be made available on request

Acknowledgments

References

[1] Atakan B, Kaiser SA, Herzler J, Porras S, Banke K, Deutschmann O, Kasper T, Fikri M, Schießl R, Schröder D, Rudolph C, Kaczmarek D, Gossler H, Drost S, Bykov V, Maas U, Schulz C. Flexible energy conversion and storage via high-temperature gas-phase reactions: The piston engine as a polygeneration reactor. Renew Sustain Energy Rev 2020;133. http://dx.doi.org/10.1016/j.rser.2020.110264.

[2] Ashok A, Katebah MA, Linke P, Kumar D, Arora D, Fischer K, Jacobs T, Al-Rawashdeh M. Review of piston reactors for the production of chemicals. Rev Chem Eng 2021. http://dx.doi.org/10.1515/revce-2020-0116.

[3] Rudolph C, Atakan B. Pyrolysis of methane and ethane in a Compression–Expansion process as a new concept for chemical energy storage: A kinetic and exergetic investigation. Energy Technol 2021;9(3):2000948. http://dx.doi.org/10.1002/ENTE.202000948.

[4] Kaczmarek D, Atakan B, Kasper T. Plug-Flow Reactor Study of the Partial Oxidation of Methane and Natural Gas at Ultra-Rich Conditions, 191 (9) (2019) 1571–1584. http://dx.doi.org/10.1080/00102202.2019.1577829.

[5] Eckart S, Yu C, Maas U, Krause H. Experimental and numerical investigations on extinction strain rates in non-premixed counterflow methane and propane flames in an oxygen reduced environment. Fuel 2021;298:120781. http://dx.doi.org/10.1016/J.FUEL.2021.120781.

[6] Luo Y, Strassacker C, Wen X, Sun Z, Maas U, Hasse C. Strain rate effects on head-on quenching of laminar premixed methane-air flames. Flow Turbul Combust 2021;106(2):631–47. http://dx.doi.org/10.1007/S10494-020-00179-1.

[7] Hegner R, Werler M, Schießl R, Maas U, Atakan B. Fuel-rich HCCI engines as chemical reactors for polygeneration: A modeling and experimental study on product species and thermodynamics. Energy Fuels 2017;31(12):14079–88.

[8] Banke K, Hegner R, Schröder D, Schulz C, Atakan B, Kaiser SA. Power and syngas production from partial oxidation of fuel-rich methane/DME mixtures in an HCCI engine. Fuel 2019;243(October 2018):97–103. http://dx.doi.org/10.1016/j.fuel.2019.01.076.

[9] Gossler H, Drost S, Porras S, Schießl R, Maas U, Deutschmann O. The internal combustion engine as a CO2 reformer. Combust Flame 2019;207:186–95. http://dx.doi.org/10.1016/j.combustflame.2019.05.031.

[10] Schröder D, Hegner R, Güngör A, Atakan B. Exergoeconomic analysis of an HCCI engine polygeneration process. Energy Convers Manage 2020;203:112085. http://dx.doi.org/10.1016/J.ENCONMAN.2019.112085.

[11] Wiemann S, Hegner R, Atakan B, Schulz C, Kaiser SA. Combined production of power and syngas in an internal combustion engine – Experiments and simulations in SI and HCCI mode. Fuel 2018;215(November 2017):40–5. http://dx.doi.org/10.1016/j.fuel.2017.11.002.

[12] Gossler H, Deutschmann O. Numerical optimization and reaction flow analysis of syngas production via partial oxidation of natural gas in internal combustion engines. Int J Hydrogen Energy 2015;40(34):11046–58. http://dx.doi.org/10.1016/j.IJHYDENE.2015.06.125.

[13] Happel J, Kramer L. Acetylene and hydrogen from the pyrolysis of methane. Ind Eng Chem 1967;59(1):39–50. http://dx.doi.org/10.1021/ie50685a008.

[14] Fau G, Gascoin N, Gillard P, Steelant J. Methane pyrolysis: Literature survey and comparisons of available data for use in numerical simulations. J Anal Appl Pyrolysis 2013;104:1–9. http://dx.doi.org/10.1016/J.JAAP.2013.04.006, URL http://www.sciencedirect.com/science/article/pii/S0165237013000831.

[15] Paxman D, Trottier S, Flynn M, Kostiuk L, Secanell M. Experimental and numerical analysis of a methane thermal decomposition reactor. Int J Hydrogen Energy 2017;42(40):25166–84. http://dx.doi.org/10.1016/J.IJHYDENE.2017.08.134.

[16] Nativel D, Shu B, Herzler J, Fikri M, Schulz C. Shock-tube study of methane pyrolysis in the context of energy-storage processes. Proc Combust Inst 2019;37(1):197–204. http://dx.doi.org/10.1016/J.PROCI.2018.06.083.

[17] Werler M, Cancino LR, Schiessl R, Maas U, Schulz C. Ignition delay times of diethyl ether measured in a high-pressure shock tube and a rapid compression machine. Proc Combust Inst 2015;35(1):259–66. http://dx.doi.org/10.1016/j.proci.2014.06.143.

[18] Drost S, Aznar MS, Schießl R, Ebert M, Chen JY, Maas U. Reduced reaction mechanism for natural gas combustion in novel power cycles. Combust Flame 2021;223:486–94. http://dx.doi.org/10.1016/j.combustflame.2020.09.029.

[19] Drost S, Werler M, Schießl R, Maas U. Ignition delay times of methane/diethyl ether (DEE) blends measured in a rapid compression machine (RCM). J Loss Prev Process Ind 2021;71:104430. http://dx.doi.org/10.1016/j.jlp.2021.104430.

[20] Drost S, Kaczmarek D, Eckart S, Herzler J, Schießl R, Fritsche C, Fikri M, Atakan B, Kasper T, Krause H, Schulz C, Maas U. Experimental investigation of ethanol oxidation and development of a reduced reaction mechanism for a wide temperature range. Energy Fuels 2021;35(18):14780–92. http://dx.doi.org/10.1021/acs.energyfuels.1c01993.

[21] Desgroux P, Gasnot L, Sochet LR. Instantaneous temperature measurement in a rapid-compression machine using laser Rayleigh scattering. Appl Phys B 1995;61:69–72.

[22] Pressure measurement & control baratron® manometer. Tech. rep., Andover, MA, USA; 2008, p. 1–2, URL https://www.mksinst.com/mam/celum/celum_assets/resources/121A-DS.pdf.

[23] Kistler. Kistler Gruppe: ThermoCOMP®-Quartz pressure sensor, type 6061B. Winterthur, Switzerland: Kistler Holding AG; 2013, p. 1–3, URL https://www.kistler.com/files/document/000-020e.pdf.

[24] Burster. Potentiometric displacement sensors. Models 8712, 8713. Tech. rep., Gernsbach, Germany; 2020, p. 1–2, URL https://www.burster.com/fileadmin/user_upload/redaktion/Documents/Products/Data-Sheets/Section_8/8712_EN.pdf.

[25] Agilent Technologies, Inc. Agilent 490 micro GC solution. Tech. rep., Santa Clara, CA, USA: Agilent Technologies, Inc.; 2017, p. 6, URL https://www.agilent.com/cs/library/datasheets/public/5991-6034EN.pdf.

[26] Agilent Technologies, Inc. Agilent 490 micro gas chromatograph. Tech. rep., Santa Clara, CA, USA / Shanghai, P.R.China: Agilent Technologies, Inc.; 2017, p. 132, URL https://www.agilent.com/cs/library/usermanuals/public/G3581-90001.pdf.

[27] Conn AR, Gould NI, Toint PL. A globally convergent augmented Lagrangian algorithm for optimization with general constraints and simple bounds. SIAM J Numer Anal 1991;28(2):545–72. http://dx.doi.org/10.1137/0728030.

[28] Conn AR, Gould N, Toint PL. A globally convergent Lagrangian barrier algorithm for optimization with general inequality constraints and simple bounds. Math Comp 1997;66(217):261–89. http://dx.doi.org/10.1090/s0025-5718-97-00777-1.

[29] Goldberg DE. Genetic algorithms in search, optimization & machine learning. 13. Boston, USA: Addison-Wesley; 1988.

[30] The MathWorks, Inc., find minimum of function using genetic algorithm - MATLAB ga. 2021, URL https://www.mathworks.com/help/gads/ga.html.

[31] Wilson D, Allen C. Application of a multi-zone model for the prediction of species concentrations in rapid compression machine experiments. Combust Flame 2016;171:185–97. http://dx.doi.org/10.1016/j.combustflame.2016.05.018, URL http://dx.doi.org/10.1016/j.combustflame.2016.05.018.

[32] Baigmohammadi M, Patel V, Nagaraja S, Ramalingam A, Martinez S, Panigrahy S, Mohamed AAES, Somers KP, Burke U, Heufer KA, Pekalski A, Curran HJ. Comprehensive experimental and simulation study of the ignition delay time characteristics of binary blended methane, ethane, and ethylene over a wide range of temperature, pressure, equivalence ratio, and dilution. Energy Fuels 2020;34(7):8808–23. http://dx.doi.org/10.1021/acs.energyfuels.0c00960.

[33] Dong S, Zhang K, Ninnemann EM, Najjar A, Kukkadapu G, Baker J, Arafin F, Wang Z, Pitz WJ, Vasu SS, Sarathy SM, Senecal PK, Curran HJ. A comprehensive experimental and kinetic modeling study of 1- and 2-pentene. Combust Flame 2021;223:166–80. http://dx.doi.org/10.1016/J.COMBUSTFLAME.2020.09.012.

[34] Dong S, Zhang K, Senecal PK, Kukkadapu G, Wagnon SW, Barrett S, Lokachari N, Panigaphy S, Pitz WJ, Curran HJ. A comparative reactivity study of 1-alkene fuels from ethylene to 1-heptene. Proc Combust Inst 2021;38(1):611–9. http://dx.doi.org/10.1016/J.PROCI.2020.07.053.

[35] El-Sabor Mohamed AA, Panigrahy S, Sahu AB, Bourque G, Curran HJ. An experimental and kinetic modeling study of the auto-ignition of natural gas blends containing C1–C7 alkanes. Proc Combust Inst 2021;38(1):365–73. http://dx.doi.org/10.1016/J.PROCI.2020.06.015.

[36] Lokachari N, Panigrahy S, Kukkadapu G, Kim G, Vasu SS, Pitz WJ, Curran HJ. The influence of iso-butene kinetics on the reactivity of di-isobutylene and iso-octane. Combust Flame 2020;222:186–95. http://dx.doi.org/10.1016/J.COMBUSTFLAME.2020.08.007.

[37] Nagaraja SS, Liang J, Dong S, Panigrahy S, Sahu A, Kukkadapu G, Wagnon SW, Pitz WJ, Curran HJ. A hierarchical single-pulse shock tube pyrolysis study of C2–c6 1-alkenes. Combust Flame 2020;219:456–66. http://dx.doi.org/10.1016/J.COMBUSTFLAME.2020.06.021.

[38] Nagaraja SS, Kukkadapu G, Panigrahy S, Liang J, Lu H, Pitz WJ, Curran HJ. A pyrolysis study of allylic hydrocarbon fuels. Int J Chem Kinet 2020;52(12):964–78. http://dx.doi.org/10.1002/KIN.21414.

[39] Nagaraja SS, Power J, Kukkadapu G, Dong S, Wagnon SW, Pitz WJ, Curran HJ. A single pulse shock tube study of pentene isomer pyrolysis. Proc Combust Inst 2021;38(1):881–9. http://dx.doi.org/10.1016/J.PROCI.2020.06.069.

[40] Panigrahy S, Liang J, Nagaraja SS, Zuo Z, Kim G, Dong S, Kukkadapu G, Pitz WJ, Vasu SS, Curran HJ. A comprehensive experimental and improved kinetic modeling study on the pyrolysis and oxidation of propyne. Proc Combust Inst 2021;38(1):479–88. http://dx.doi.org/10.1016/J.PROCI.2020.06.320.

[41] Ramalingam A, Panigrahy S, Fenard Y, Curran H, Heufer KA. A chemical kinetic perspective on the low-temperature oxidation of propane/propene mixtures through experiments and kinetic analyses. Combust Flame 2021;223:361–75. http://dx.doi.org/10.1016/J.COMBUSTFLAME.2020.10.020.

[42] Wu Y, Panigrahy S, Sahu AB, Bariki C, Beeckmann J, Liang J, Mohamed AA, Dong S, Tang C, Pitsch H, Huang Z, Curran HJ. Understanding the antagonistic effect of methanol as a component in surrogate fuel models: A case study of methanol/n-heptane mixtures. Combust Flame 2021;226:229–42. http://dx.doi.org/10.1016/J.COMBUSTFLAME.2020.12.006.

[43] Marinov NM, Pitz WJ, Westbrook CK, Vincitore AM, Castaldi MJ, Senkan SM, Melius CF. Aromatic and polycyclic aromatic hydrocarbon formation in a laminar premixed n-butane flame. Combust Flame 1998;114(1–2):192–213. http://dx.doi.org/10.1016/S0010-2180(97)00275-7.

[44] Maas U, Warnatz J. Ignition processes in hydrogen-oxygen mixtures. Combust Flame 1988;74(1):53–69. http://dx.doi.org/10.1016/0010-2180(88)90086-7.

[45] Deng J, Bae C, Denlinger A, Miller T. Electric vehicles batteries: Requirements and challenges. Joule 2020;4(3):511–5. http://dx.doi.org/10.1016/j.joule.2020.01.013, URL https://www.sciencedirect.com/science/article/pii/S254243512030043X.

[46] Nagel B, Dellweg H, Gierasch LM. Glossary for chemists of terms used in biotechnology. Pure Appl Chem 1992;64(1):143–68.